Probes of spin conservation in heavy metal reactions: Experimental and theoretical studies of the reactions of Re^+ with H_2, D_2, and HD

P. B. Armentrout[a] and Feng-Xia Li
Department of Chemistry, University of Utah, Salt Lake City, Utah 84112-0850

(Received 6 April 2004; accepted 13 April 2004)

A guided ion beam tandem mass spectrometer is used to examine the kinetic energy dependence of reactions of the third-row transition metal cation, Re^+, with molecular hydrogen and its isotopologues. A flow tube ion source produces Re^+ in its $^7S_3$ electronic ground state. Reaction with H_2, D_2, and HD forms $ReH^+(ReD^+)$ in endothermic processes. Modeling of the endothermic reaction cross sections yields the 0 K bond dissociation energy of $D_0(Re^+–H)=2.29\pm0.07$ eV (221 ± 6 kJ/mol). The experimental thermochemistry is consistent with *ab initio* calculations, performed here and in the literature. Theory also provides the electronic structures of these species and is used to examine the reactive potential energy surfaces. Results from reactions with HD provide insight into the reaction mechanisms and indicate that the late metal ion, Re^+, reacts largely via a statistical mechanism. This is consistent with the potential energy surfaces which locate a stable $ReH_2^+(^5B_2)$ complex. Results for this third-row transition metal system are compared with the first-row congener (Mn^+) and found to have much higher reactivity towards dihydrogen and stronger $M^+–H$ bonds. These differences can be attributed to efficient coupling among surfaces of different spin along with lanthanide contraction and relativistic effects. © *2004 American Institute of Physics.* [DOI: 10.1063/1.1758695]

I. INTRODUCTION

Insight into the activation of covalent bonds, important processes in many homogeneous and heterogeneous catalytic processes,[1,2] can be obtained in many ways. Among the simplest, and therefore potentially among the most valuable because it can be studied in detail both experimentally and theoretically, is the activation of dihydrogen at single metal centers. The periodic trends in this chemistry are particularly interesting[3,4] and there are now numerous experimental studies of the reactions of the ions of atomic first-row transition metals,[5–15] second-row transition metals,[14–18] third-row transition metals,[16,19,20] and other metals[21–25] with dihydrogen, reaction (1), and its isotopic analogues

$$M^+ + H_2 \rightarrow MH^+ + H. \quad (1)$$

In addition to the kinetics and dynamics of this reaction, the guided ion beam methods used in our laboratory can also investigate the bond dissociation energies (BDEs) for $M^+–H$ by analysis of the kinetic energy dependence of reaction (1).[26–28] Such thermochemistry is of obvious fundamental interest and has implications for understanding a variety of catalytic reactions involving transition metal systems.[1,2]

We are presently engaged in a systematic study of reaction (1) for the third-row transition-metal cations. Previously, La^+,[16] Lu^+,[16] Ta^+,[19] W^+,[19] and Pt^+[20] have been studied experimentally, and theoretical studies include all of the third-row transition-metal cations.[29–36] We continue these studies here by reporting absolute cross sections as a function of kinetic energy for reactions of H_2 and D_2 with Re^+ and analyze them to acquire $D_0(Re^+–H)$. Detailed theoretical calculations on the ReH^+ and ReH_2^+ species were also performed to assign electronic structures and explore possible mechanisms. These are compared to the previous results of Ohanessian *et al.*[29] for ReH^+ and Dai and Balasubramanian[32] for ReH_2^+. To provide additional information about the reaction mechanisms, we also study the reactions of Re^+ with HD over a wide range of kinetic energies. Such reactions with HD have previously been shown to provide useful mechanistic information.[3,4,11,14,16–18] Finally, we compare the reactivities and mechanisms of Re^+ with its first-row congener, Mn^+.[11]

II. EXPERIMENT

A. General procedures

The guided ion beam tandem mass spectrometer on which these experiments were performed has been described in detail previously.[37,38] Briefly, atomic metal ions are generated in a direct current discharge flow tube source described below, extracted from the source, accelerated, and focused into a magnetic sector momentum analyzer for mass selection of primary ions. The mass-selected ions are decelerated to a desired kinetic energy and focused into an octopole ion beam guide that uses radio-frequency electric fields to trap the ions in the radial direction and ensure complete collection of reactant and product ions.[39,40] The octopole passes through a static gas cell with an effective length of 8.26 cm that contains the reaction partner at a low pressure (usually less than ~0.3 mTorr) so that multiple ion–molecule collisions are improbable. All products reported here result from single bimolecular encounters, as verified by

[a]Author to whom correspondence should be addressed. Electronic mail: armentrout@chem.utah.edu

pressure dependence studies. The unreacted parent and product ions are confined radially in the guide until they drift to the end of the octopole where they are extracted, focused, and passed through a quadrupole mass filter for mass analysis of products. Ions are subsequently detected with a secondary electron scintillation ion detector using standard pulse counting techniques. Reaction cross sections are calculated from product ion intensities relative to reactant ion intensities after correcting for background signals.[41] Uncertainties in absolute cross sections are estimated to be ±20%.

The kinetic energy of the ions is varied in the laboratory frame by scanning the dc bias on the octopole rods with respect to the potential of the ion source region. Laboratory (lab) ion energies are converted to energies in the center-of-mass frame (c.m.) by using the formula $E_{CM}=E_{lab}\,m/(m+M)$, where m and M are the neutral and ionic reactant masses, respectively. Two effects broaden the cross section data: the kinetic energy distribution of the reactant ion and the thermal motion of the neutral reactant gas (Doppler broadening).[42] The absolute zero and the full width at half maximum (FWHM) of the kinetic energy distribution of the reactant ions are determined using the octopole beam guide as a retarding potential analyzer, as described previously.[41] The distributions of ion energies, which are independent of energy, are nearly Gaussian and have a typical FWHM of 0.4–0.9 eV (lab) in these studies. These values are somewhat larger than is usual for this instrument in part because of the extremely wide energy range needed in these studies (lab energies from 0 to 800 eV). This requires different focusing of the ion beam than is optimal for determining the zero of energy and energy distributions. Uncertainties in the absolute energy scale are ±0.05 eV (lab).

B. Ion source

Atomic metal ions are produced in a direct current discharge flow tube (dc/FT) source,[38] consisting of a cathode held at high negative voltage (0.7–1.5 kV) over which a flow of approximately 90% He and 10% Ar passes at a total pressure of 0.3–0.5 Torr and ambient temperature. In this work, the cathode is a rhenium cylinder attached to an iron holder. Ar^+ ions created in the discharge are accelerated toward the metal cathode, thereby sputtering Re^+ cations, which are then swept down a 1 m long flow tube. The ions undergo $\sim 10^5$ thermalizing collisions with He and $\sim 10^4$ collisions with Ar before entering the guided ion beam apparatus. Generally, these conditions are sufficient to produce atomic ions in their ground electronic state. However, trace amounts of low-lying excited states of Re^+ are observed to survive these flow conditions, as found by examining the test reaction of Re^+ with CH_4.[43] In this study, there is evidence that the excited states comprise less than 0.1% of the beam. These excited species are easily removed by introducing CH_4 to the flow tube about 15 cm downstream of the discharge zone at a pressure of ~100 mTorr.[43]

With the addition of this cooling gas, the dc/FT source produces metal ions in the ground state. For example, on the basis of comparisons to a surface ionization source, the dc/FT source was found to generate Sc^+,[44] Fe^+,[45] Co^+,[46] Ni^+,[47] Ru^+,[17] Rh^+,[17] and Pd^+[17] ions with an average electronic temperature of 700±400 K, and Y^+, Zr^+, Nb^+, and Mo^+ ions with an average electronic temperature of 300 ±100 K.[18] In the case of Re^+, even an elevated electronic temperature produces a pure beam of $^7S_3$ ground state, because excited states are much too high in energy to be populated. The ^5D first excited state has an average energy of 1.827 eV with the ^5S second excited state at 2.135 eV.[48]

C. Data analysis

The kinetic-energy dependence of product cross sections is analyzed to determine E_0, the energy threshold for product formation at 0 K. E_0 differs from the apparent threshold observed under laboratory conditions because of the Maxwell–Boltzmann velocity distribution and internal energy of the neutral reactants, and the kinetic distribution of the reactant ions. Each of these contributions allows reactions to occur at energies below E_0. To determine E_0, endothermic reaction cross sections are modeled using Eq. (2),[26–28,49–52]

$$\sigma(E)=\sigma_0\Sigma g_i(E+E_{el}+E_i-E_0)^n/E, \quad (2)$$

where σ_0 is an energy-independent scaling factor, E is the relative kinetic energy of the reactants, E_{el} is the electronic energy of the metal cation, and n is an adjustable parameter. The sum considers contributions from rovibrational states of the neutral reactants at 300 K, denoted by i, having energies E_i and populations g_i, where $\Sigma g_i=1$. As noted above, E_{el} is believed to be 0.0 eV for Re^+. The various sets of vibrational frequencies and rotational constants used to determine E_i in this work are taken from the literature for H_2, D_2, and HD.[53] Before comparison with the experimental data, Eq. (2) is convoluted with the kinetic energy distributions of the atomic ions and neutral reactants at 300 K. The σ_0, n, and E_0 parameters are then optimized using a nonlinear least-squares analysis to give the best reproduction of the data.[41] Error limits for E_0 are calculated from the range of threshold values for different data sets over a range of acceptable n values combined with the absolute errors in the kinetic energy scale.

III. THEORETICAL CALCULATION SECTION

Most quantum chemistry calculations reported here are computed using the B3LYP hybrid density functional method,[54,55] and performed with the GAUSSIAN 98 suite of programs.[56] A large basis set is used for hydrogen, triple zeta with diffuse and polarization functions, 6-311+G(3p). This basis set gives good results for the thermochemistry of dihydrogen, with deviations from experiment of less than 0.03 eV for the bond energy of H–H (4.505 eV calculated versus 4.478 eV experimental).[53] The 60 core electrons of rhenium are described by the relativistic effective core potentials (ECPs) of Hay–Wadt (HW),[57] with valence electrons described by the Los Alamos double zeta basis set (LANL2DZ). This basis set is optimized for neutral atoms, whereas the positive charge differentially contracts the s orbitals compared to the d orbitals. Hence, all calculations were performed with an altered HW–ECP basis for Re^+ as described by Ohanessian *et al.* (HW+).[29] In all cases, the

thermochemistry calculated and cited here is corrected for zero point energy effects, after scaling the frequencies by 0.9804.[58]

Holthausen *et al.*[59] carefully considered the most appropriate choice for a level of theory for the first and third row transition metal methyl cations, species analogous to the metal hydride cations considered here, because both have single covalent metal–ligand bonds. These authors used B3LYP, Becke-half-and-half-LYP (BHLYP), and QCISD(T) methods with a basis set consisting of a polarized double-ζ on C and H and the Hay/Wadt relativistic ECP with valence electrons added. The symmetries of the metal methyl species were constrained to C_{3v}. Upon comparison with experimental results for the first row MCH_3^+ species (M=Sc–Cu),[26,27] these authors conclude that the B3LYP functional overbinds severely, whereas the BHLYP functional and the QCISD(T) methods perform more accurately. Mean average deviations (MADs) from experiment were 0.41, 0.18, and 0.20 eV, respectively. Likewise, the bond energies calculated using B3LYP were higher than those for BHLYP and QCISD(T) for the third row metal methyl cations. Given these results, we also performed calculations for the ReH^+ species using QCISD(T), the BHLYP functional, and the Stuttgart/Dresden (SD) ECP[60] for Re^+. Such calculations will be explicitly noted and unless otherwise designated, our results will refer to a B3LYP/HW+/6-311+G(3p) level of theory. For ReH_2^+ species where multiple bonds to Re^+ are formed, only the B3LYP functional is used. This choice is rationalized on the basis of the results of Holthausen *et al.*[61] for metal–methylene cations and our own studies of $ReCH_x^+$ ($x=0-2$) species.[43]

At the B3LYP/HW+ level of theory, we calculate a ^7S ground state for Re^+, with quintet states at 1.372 and 2.104 eV, a triplet state at 2.265 eV, and a singlet state at 5.583 eV. The excitation to the lowest lying quintet state was found to be 1.380, 1.493, and 1.484 eV for the B3LYP/SD, BHLYP/HW+, and BHLYP/SD combinations of theory/basis set, showing that the atomic excitations are not strongly dependent on the choices made between density functionals and ECP. However, at the QCISD(T)/HW+ level of theory, the first quintet is found at 2.326 eV. In all cases, the first quintet state exhibits spin contamination ($s^2=6.95$ rather than 6.0) and clearly contains some $6s^15d^5$ character, whereas the second value appears to be pure $5d^6$ (^5D)($s^2=6.0$). These septet–quintet excitation energies are roughly comparable with the experimental excitation energies of 1.827 for the ^5D first excited state and 2.135 for the ^5S second excited state.[48] Excitation energies for triplet and singlet states of Re^+ have not been experimentally identified largely because of the extensive spin–orbit coupling for this heavy metal. The difficulties associated with accurate calculations of the various spin states of a heavy metal like Re^+ are illustrated by excitation energies given in the literature. Ohanessian *et al.* calculate a ^7S ground state with a $^5D(5d^6)$ state at 2.64 eV and a $^5D(6s^25d^4)$ state at 2.94 eV.[29] Dai and Balasubramanian calculated an excited $^5G(5d^6)$ state lying at 2.687 eV, with triplet and singlet states at 4.182 and 4.377 eV, respectively.[32] Oddly, the calculations of Holthausen *et al.*[59] find a ground state of $^5D(5d^6)$ using the B3LYP and BHLYP functionals, with the ^7S state lying 0.26 and 0.10 eV higher in energy. Their QCISD and QCISD(T) calculations provided the correct ordering with quintet excitation energies of 1.11 and 1.09 eV, respectively. The lack of agreement among any of these calculations is surprising and disappointing.

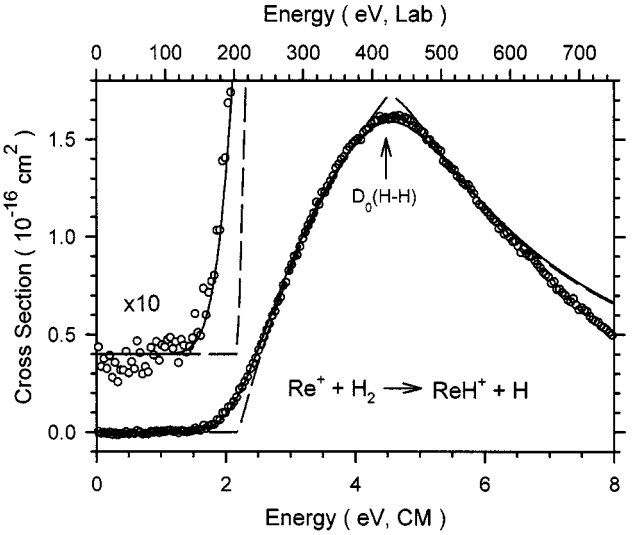

FIG. 1. Cross sections for reaction of $Re^+(^7S)$ with H_2 as a function of kinetic energy in the center-of-mass frame (lower axis) and laboratory frame (upper axis). The best fit of Eq. (2) with parameters of Table I to the data is shown as a dashed line. The solid line shows this model convoluted over the kinetic and internal energy distributions of the reactant neutral and ion. The arrow indicates D_0(H–H) at 4.478 eV.

IV. EXPERIMENTAL RESULTS

A. Reactions with H_2 and D_2

Figures 1 and 2 show cross sections as a function of kinetic energy for the bimolecular reaction of H_2 and D_2

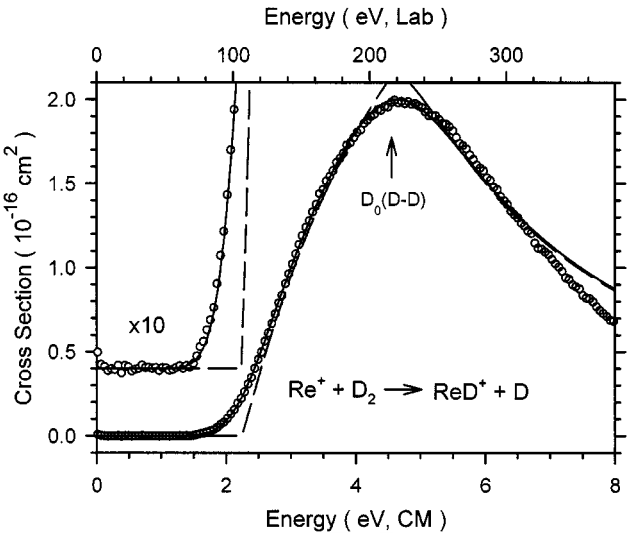

FIG. 2. Cross sections for reaction of $Re^+(^7S)$ with D_2 as a function of kinetic energy in the center-of-mass frame (lower axis) and laboratory frame (upper axis). The best fit of Eq. (2) with parameters of Table I to the data is shown as a dashed line. The solid line shows this model convoluted over the kinetic and internal energy distributions of the reactant neutral and ion. The arrow indicates D_0(D–D) at 4.556 eV.

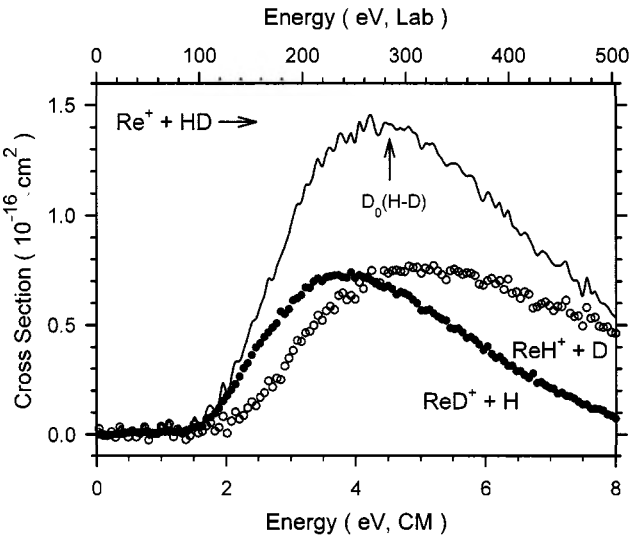

FIG. 3. Cross sections for reaction of $Re^+(^7S)$ with HD as a function of kinetic energy in the center-of-mass frame (lower axis) and laboratory frame (upper axis). The arrow indicates D_0(H–D) at 4.51 eV.

with Re^+ produced in the dc/FT source with methane added to quench residual excited states. Reaction (1) and its deuterated analogue are the only processes observed. Results for the reaction $Re^+ + D_2$ can be easier to acquire because the heavier isotope reduces mass overlap between the product ion and the much more intense primary ion, thereby allowing intensities of the product ion to be measured more accurately over a larger dynamic range. However, the same mass resolution conditions were used to collect data for the H_2, D_2, and HD systems here. The absolute magnitudes of the $Re^+ + H_2$ and $Re^+ + D_2$ reaction cross sections differ by about 20%, comparable to the estimated 20% experimental uncertainty, and the energy dependences of the cross sections for the two systems are quite consistent.

The cross sections rise from apparent thresholds near 1.5 eV and reach maxima near the dissociation energy of H_2, $D_0(H_2) = 4.478$ eV, or D_2, $D_0(D_2) = 4.556$ eV.[53] At higher energies, the $ReH^+(ReD^+)$ products can be formed with internal energies in excess of the bond dissociation energy, such that these products begin to dissociate in the overall reaction (3)

$$Re^+ + H_2(D_2) \rightarrow ReH^+(ReD^+) + H(D) \rightarrow Re^+ + 2H(D). \quad (3)$$

The observation that the experimental cross sections reach maxima very close to the $H_2(D_2)$ bond energies illustrates that these processes begin promptly at their thermodynamic threshold.

B. Reactions with HD

Re^+ reacts with HD to yield both ReH^+ and ReD^+ in reactions (4) and (5), Fig. 3

$$Re^+ + HD \rightarrow ReH^+ + D \quad (4)$$

$$\rightarrow ReD^+ + H. \quad (5)$$

Because of the close proximity of the product masses, there can easily be some overlap between these signals depending on the mass resolution used in the quadrupole mass filter. In the present system, it was carefully checked that high resolution leading to separation of these products could be used without sacrificing efficient collection of the product ions. The accuracy of the final results is confirmed by good agreement between the magnitudes of the total cross sections for the HD system and those of the H_2 and D_2 systems (Figs. 1 and 2).

The total cross section in the HD system exhibits endothermic behavior and rises from an apparent threshold that is similar to those of the H_2 and D_2 systems. The total cross section reaches a maximum near the bond dissociation energy of HD, 4.51 eV.[53] The individual ReH^+ and ReD^+ cross sections behave somewhat differently with energy such that the ReD^+ cross sections rise more rapidly from an earlier apparent onset and then peak at somewhat lower energies than those of ReH^+. This behavior can be rationalized because the $ReD^+ + H$ product channel has a lower energy threshold by the zero point energy difference of 0.037 eV (see below). It is somewhat surprising that this introduces such a strong preference for this channel but it can be seen from the slow onset in the ReH^+ cross sections that this channel suffers from competition with the energetically favored ReD^+ channel. In contrast, at higher energies, the ReD^+ cross section declines at an energy before the onset of dissociation because of competition with the $ReH^+ + D$ channel. This observation shows that the ReH^+ product ion is stabilized by removal of energy by the D atom product relative to $ReD^+ + H$. The relative high-energy behavior shows that the D atom carries away more energy from ReH^+ than the H atom carries away from ReD^+. This effect is typical of atomic ion reactions with H_2, HD, and D_2,[4,14,17,18] and has been discussed in detail elsewhere.[4,62–64]

V. THERMOCHEMICAL AND THEORETICAL RESULTS

A. Thermochemistry

The endothermic cross sections in the H_2 and D_2 reaction systems are analyzed in detail using Eq. (2). Typical models are shown in Figs. 1 and 2 and can be seen to reproduce the experimental results very well until about 6 eV. At energies above $D_0(H_2)$ and $D_0(D_2)$, where reaction (3) can begin, the analyses include a model for this subsequent dissociation, as outlined in detail elsewhere.[65] This high energy model requires two parameters: E_D fixes the onset for $ReH^+(ReD^+)$ dissociation in reaction (3), and the exponent p determines the energy dependence [similar to n in Eq. (2)]. For the results shown in Figs. 1 and 2, E_D is fixed to the $H_2(D_2)$ bond energy and the optimum value of p was found to be 1.0.

The optimum values of the parameters in Eq. (2) for these systems are listed in Table I. These values represent the average of at least seven data sets for each system. As can be seen in Figs. 1 and 2, the optimum values of E_0 differ appreciably from the apparent thresholds, which is largely a result of the appreciable velocity distribution of the light $H_2(D_2)$ reactant. Because the convoluted form of Eq. (2) includes all sources of energy (rotational, vibrational, translational, and electronic energy distributions of reactants are

TABLE I. Parameters of Eq. (2) used in modeling reaction (1) and its deuterated analogue and the resultant bond energies.

Reaction	σ_0	n	E_0 (eV)	$D_0(Re^+-H)$ (eV)
$Re^+ + H_2$	2.9±0.2	1.1±0.1	2.17±0.04	2.30±0.04
$Re^+ + D_2$	4.0±0.3	1.1±0.1	2.25±0.06	2.27±0.06[a]

[a]Value corrected for the zero-point energy difference of 0.037 eV. See text.

explicitly included in the modeling), the E_0 threshold energies determined correspond to 0 K values. From the thresholds measured, the BDEs for the metal–ligand cations observed in reaction (1) can be calculated using Eq. (6) and an analogous equation for the deuterated system

$$D_0(Re^+-H) = D_0(H_2) - E_0, \quad (6)$$

where $D_0(H-H) = 4.478$ eV and $D_0(D-D) = 4.556$ eV.[53] This equation assumes that there is no activation barrier in excess of the endothermicity of the reaction, an assumption that is often true for ion–molecule reactions because of the long-range attractive forces[51] and one that can be tested using theory; see below. A summary of the Re^+–H bond energies derived from the present experiments with both H_2 and D_2 is given in Table I. This includes adjusting the value for $D_0(Re^+-D)$ for the zero point energy difference between ReD^+ and ReH^+. This correction uses a vibrational frequency of 2050 cm^{-1} for ReH^+, and 1454 cm^{-1} for ReD^+ calculated here for the $^6\Sigma^+$ state (Table II), a value in excellent agreement with a 2065 cm^{-1} value calculated by Ohanessian *et al.* for ReH^+.[29] Thus the zero point energy differences in the ReH^+ and ReD^+ bond energies are 0.037 ±0.004 eV, assuming a 10% uncertainty in the frequency. The Re^+–H bond energies obtained from the H_2 and D_2 systems are in excellent agreement with one another (Table I). Our best value for this bond energy is the weighted average of these two values, 2.29±0.07 eV (221±6 kJ/mol), where the uncertainty is 2 s.d.

B. ReH^+ theoretical bond energy

Generalized valence bond (GVB) calculations indicate that the Re^+–H bond in the $^6\Sigma^+$ ground state is formed by covalent interaction between a $6s-5d\sigma$ hybrid (57% $5d$ and 42% $6s$) and the singly occupied $1s$ orbital on H.[29] Formation of this bond requires spin decoupling of the bonding electron from the remaining nonbonding electrons, which involves loss of spin exchange energy. This exchange correction for the high-spin state of $Re^+(^7S)$ is at a maximum among the third-row transition metal cations, 0.33 eV. The nonbonding orbitals singly occupy metal-based π and δ orbitals along with the other $6s-5d\sigma$ hybrid. GVB theory followed by correlation consistent configuration interaction calculations[29] provides a BDE for ReH^+ of 1.93 eV, somewhat lower than the experimental result of 2.29±0.07 eV.

Our calculations also find a $^6\Sigma^+$ ground state for ReH^+. Bond lengths for the B3LYP/HW+, B3LYP/SD, BHLYP/HW+, and BHLYP/SD calculations are in good agreement: 1.647, 1.655, 1.647, and 1.652 Å, and agree well with that from Ohanessian *et al.*, 1.659 Å.[29] In contrast, the 0 K bond energies are quite dependent on the level of theory used. For the B3LYP functional, the HW+ and SD ECPs provide bond energies (zero point energy corrected) of 2.62 and 2.54 eV, respectively, whereas the BHLYP functional gives 2.38 and 2.32 eV, respectively. Thus, as found by Holthausen *et al.*,[59] the B3LYP overbinds by several tenths of an electron volt, whereas the BHLYP functional provides fairly accurate bond energies compared to experiment for this singly bonded metal–ligand species. We also calculated a value at the QCISD(T)/HW+/6-311+G(3p) level (using the B3LYP/HW+/6-311+G(3p) geometry), 2.24 eV, in good agreement with experiment.

TABLE II. Theoretical geometries and energies for ReH^+.[a]

Species	r_e(Re–H) (Å)	E_{rel} (eV)[b]	Frequencies (cm^{-1})[c]
$ReH^+(^6\Sigma^+)$	1.647	0.000	2050
$(^4\Sigma^+)$	1.636	1.625	2092
$(^2\Pi)$	1.631	1.846	2180
$(^4\Pi)$	1.628	1.946	2109
$(^4\Delta)$	1.647	2.085	2087
$(^2\Delta)$	1.640	2.954	2106
$(^2\Sigma^+)$	1.669	3.157	2018
$(^6\Pi)$	1.839	4.649	1422
$(^6\Delta)$	1.796	5.222	1538

[a]Results of B3LYP/HW+/6-311+G(3p) calculations.
[b]Energies relative to the ground state including zero point energies.
[c]Vibrational frequencies scaled by 0.9804. Value for $ReH^+(^6\Sigma^+)$ calculated by Ohanessian *et al.* (Ref. 29) is 2065 cm^{-1}.

C. ReH^+ excited states

Previous work has not investigated excited states of ReH^+. Here we used B3LYP/HW+/6-311+G(3p) to characterize several excited states. These are listed in Table II. As noted above, the $^6\Sigma^+$ state has a $\sigma_b^2\sigma^1\pi^2\delta^2$ valence configuration, where σ_b represents the bonding orbital and the remaining are nonbonding orbitals on the metal. To a first approximation, the $^4\Sigma^+$ first excited state and $^2\Sigma^+$ state also have this configuration with different coupling among the electrons. Likewise, the $^{4,2}\Pi$ states can be viewed as having $\sigma_b^2\sigma^0\pi^3\delta^2$ configurations and the $^{4,2}\Delta$ states as having $\sigma_b^2\sigma^0\pi^2\delta^3$ configurations. In order to maintain high spin, the $^6\Pi$ and $^6\Delta$ states require that an electron be excited into an antibonding orbital, whereas all other states identified correspond to alternate electron configurations of the nonbonding orbitals. Thus, all of the low-lying states have bond lengths comparable to the ground state, ranging from 1.628 to 1.669 Å, except for the $^6\Pi$ and $^6\Delta$ states, which have bond lengths near 1.8 Å. Not surprisingly, occupation of the antibonding orbital also leads to appreciable excitation energies for the latter two states (Table II).

D. ReH_2^+ states

To explore coarse features of the potential energy surface for reaction (1), we also calculated the properties of stable ReH_2^+ complexes (Table III). Our results can be compared directly with those of Dai and Balasubramanian (DB), who calculated potential energy surfaces (PESs) for interaction of several spin states of Re^+ with H_2 at the complete active space self-consistent field (CASSCF) level.[32] Single point

TABLE III. Theoretical geometries and energies for ReH_2^+.

Species	This work[a]				Literature[b]		
	r_e(Re–H) (Å)	∠H Re H (°)	E_{rel} (eV)[c]	Frequency (cm^{-1})[d]	r_e(Re–H) (Å)	∠H Re H (°)	E_{rel} (eV)[c]
$ReH_2^+(^5B_2)$	1.637	95.0	0.000	375, 2096, 2112	1.674, 1.642	95.6, 92.3	0.0, 0.0
$(^7A_1)$	2.783	15.5	0.535	174, 269, 4201	⋯	⋯	⋯
$(^3B_2)$	1.632	94.5	1.058	345, 2127, 2144	1.659, 1.627	106.9, 101.2	1.47, 1.87
					1.649, 1.620	72.6, 76.0	2.03, 1.87
$(^3B_1)$	1.626	106.9	1.781	654, 2124, 2150	1.648, 1.614	72.9, 74.4	2.07, 2.00
$(^3A_2)$	1.615	70.6	1.786	543, 2136, 2172	1.658, 1.623	106.2, 105.3	2.04, 1.98
$(^3A_1)$	1.628	100.7	2.254	467, 1964, 2152	1.666, 1.630	94.2, 90.2	2.59, 2.51
$(^1A_1)$	1.632	86.8	2.756	212, 2136, 2167	1.649, 1.614	89.4, 74.4	2.72, 2.61
$(^5A_1)$	1.707	144.6	2.819	868, 1930, 1996	1.748, 1.733	153.5, 147.4	3.21, 3.12
$(^5A_2)$	2.503	17.5	3.362	318, 321, 4048	⋯	⋯	⋯
	1.716	142.8	3.362	829, 1860, 1995	1.750, 1.728	149.2, 146.9	3.61, 3.16
$(^5B_1)$	2.523	17.3	3.399	225, 304, 4096	⋯	⋯	⋯
	1.699	142.7	3.572	838, 1931, 1989	1.728, 1.706	144.3, 143.5	4.00, 3.43

[a]Calculations using B3LYP/HW+/6-311+G(3p).
[b]CASSCF, MRSDCI values from Dai and Balasubramanian (Ref. 32).
[c]Energies relative to the ground state including zero point energies.
[d]Vibrational frequencies scaled by 0.9804.

calculations on the stationary points were then conducted at a multireference single and double configuration interaction (MRSDCI) level. These calculations use a relativistic effective core potential on Re that retains the ns and $(n-1)d$ orbitals in the valence space. In all of these calculations (ours and those of DB), the symmetry was restricted to C_{2v} and excited surfaces having the same symmetry as lower energy surfaces were not included in the work.

For ReH_2^+, our B3LYP/HW+/6-311+G(3p) calculations find an inserted $^5B_2$ ground state with a 0 K BDE of 0.66 eV relative to the $Re^+(^7S)+H_2$ asymptote. QCISD(T)/HW+/6-311+G(3p) calculations were also carried out at the B3LYP geometry and find $D_0(Re^+–H_2)=0.13$ eV ($D_e=0.15$ eV), somewhat weaker than the B3LYP values but still bound compared to the reaction asymptote. Dai and Balasubramanian also find that the $^5B_2$ is the lowest state for ReH_2^+, however, relative to the $Re^+(^7S)+H_2$ asymptote, they calculate it is unbound by 0.74 and 0.22 eV at the CASSCF and MRSDCI levels of theory, and 0.17 eV for a full second-order configuration interaction (SOCI) calculation. Relative to their $Re^+(^5G)+H_2$ asymptote, they find the $^5B_2$ state is bound by 2.12 eV (MRSDCI and SOCI), compared to our calculations which find 2.03 (B3LYP) and 2.46 (QCISD(T)) eV BDEs relative to the quintet state asymptote. Thus, the main difference between the calculations of DB and those conducted here appears to be primarily a difference in the asymptotic limits. This is further confirmed by comparing the excitation energies for the various quintet and triplet states of ReH_2^+ given in Table III. For instance, the MRSDCI excitation energies for seven different quintet and triplet excited states (all but the $^3B_2$) differ from those calculated here by a MAD of 0.21±0.06 eV (the MAD for the CASSCF values is 0.28±0.13 eV). The $^3B_2$ state differs much more, by 0.8 eV (MRSDCI), for reasons that are unclear. The geometries (bond lengths and angles) in the present B3LYP calculations are comparable to those of Dai and Balasubramanian in all cases, although it appears the identification of the $^3B_1$ and $^3A_2$ states (which lie very close in energy) may be switched. Bond lengths agree very nicely between the present calculations and the MRSDCI results of DB (MAD of 0.011±0.008 Å for nine states, all but $^7A_1$), whereas the CASSCF results differ more appreciably (MAD of 0.032±0.009 Å for nine states, all but $^7A_1$). Bond angles also agree well with MADs of 5°±4° for both the MRSDCI and CASSCF results.

We also identified several states corresponding to intact dihydrogen molecules weakly bound to Re^+. These states are identified by long Re^+–H bond lengths, 2.5–2.8 Å, and by small H Re H bond angles, 15°–18°. The covalently bound dihydrides have bond lengths between 1.6 and 1.7 Å and bond angles of 70°–150° (Table III). Not surprisingly, the only septet spin state found ($^7A_1$) involves one of these $Re^+(H_2)$ structures, but $^5A_2$ and $^5B_1$ states were also identified. All other quintet and triplet states evolve along surfaces in which Re^+ spontaneously inserts into the dihydrogen molecule to form a dihydride, as detailed in the next section. Dai and Balasubramanian also identified several more singlet states in their calculations ($^1A_2$, $^1B_1$, and $^1B_2$), which lie 0.5–1.0 eV above the $^1A_1$ and were not looked for here.

E. $Re^+ + H_2$ reaction surfaces

The complete surfaces for the various ReH_2^+ states as a function of bond angle are shown in Fig. 4. These were obtained from relaxed PES scan calculations starting at the optimized geometry of each state. The character of these surfaces is generally comparable to those found by Dai and Balasubramanian, including the complicated shapes of the higher-lying quintet excited surfaces. Two key differences are found between the calculations. First, as noted above, the energies of the surfaces relative to the $Re^+(^7S)+H_2$ asymptote are lower here. Second, the character of the $^3B_2$ surface is quite different. We find that the $^3B_2$ surface parallels the $^5B_2$ surface quite closely, which seems reasonable if the only difference between the two is the spin coupling of the nonbonding electrons. In contrast, DB find that the $^3B_2$ surface

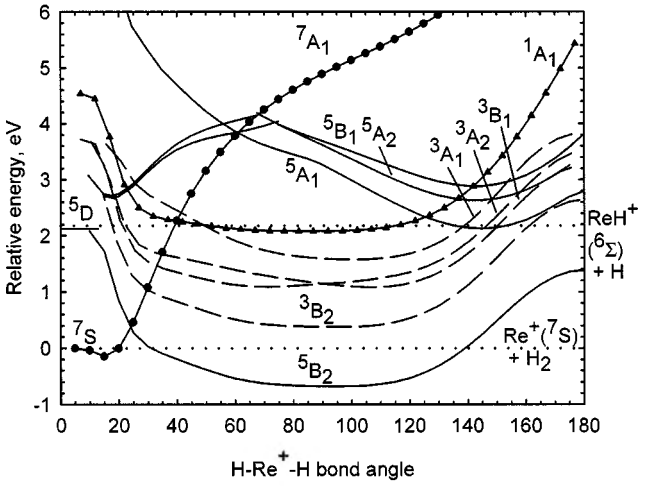

FIG. 4. B3LYP/HW+6-311+G(3p) calculations of the potential energy surfaces for the interaction of Re^+ with H_2 in C_{2v} symmetry as a function of the H–Re^+–H bond angle in degrees. Dotted lines indicate the experimental energy zero, corresponding to the $Re^+(^7S)+H_2$ reactants at 0.0 eV, and the experimental energy of the $ReH^+(^6\Sigma^+)+H$ products, 2.18 eV above the reactants.

closely follows the lower of the $^3A_2$ and $^3B_1$ surfaces. This double-welled potential (Table III) is not found here.

Because of the C_{2v} symmetry restriction, the PESs in Fig. 4 and those of DB cannot examine the $ReH^+ + H$ dissociation asymptote. It seems likely that these products can be formed from the ReH_2^+ intermediates with no barriers in excess of the endothermicity for the following reasons. The $^6\Sigma^+$ ground state of ReH^+ can interact with $H(^2S)$ to form both a high-spin septet state and a low-spin quintet state of ReH_2^+. Formation of the high-spin state would be largely repulsive as no bond formation is involved, but along the quintet surface, covalent coupling of a nonbonding $ReH^+(^6\Sigma^+)$ electron with H occurs, such that the surface should be strongly attractive. To verify this hypothesis, we performed relaxed potential energy surface scans at the B3LYP/HW+/6-311+G(3p) level starting with the bound $ReH_2^+(^5B_2)$ species and systematically lengthening one of the Re–H bonds along a $^5A'$ surface. As this bond length increases, the bond angle, which starts at 95°, gradually opens to about 125° and leads directly to $ReH^+(^6\Sigma^+)+H$ products with no barriers in excess of the endothermicity.

We also considered a collinear reaction between Re^+ and H_2. Qualitatively, this may be reasonable as the single $6s$ electron on $Re^+(^7S)$ makes it similar to $H(^2S)$, which is known to react most efficiently with H_2 along a collinear $C_{\infty v}$ path, rather than a perpendicular C_{2v} path. Indeed, we find that the collinear pathway is a viable reaction pathway. Initial approach of $Re^+(^7S)$ to H_2 is slightly attractive and leads to a well approximately 0.13 eV deep (no zero point corrections), approximately the same as the potential well for the $^7A_1$ state of ReH_2^+ (Table III). The Re^+–H–H adduct has a Re–H bond length of 2.457 Å and an H–H bond length of 0.752 Å, similar to that calculated for free H_2, 0.743 Å. From this adduct, lengthening the H–H bond leads to $ReH^+(^6\Sigma^+)+H$ products with no barrier. This product asymptote can also follow a quintet surface, forming a $ReHH^+$ species having a Re–H bond length of ~2.50 Å and an H–H bond length of 0.75 Å. This species lies 0.11 eV below the $Re^+(^5S)+H_2$ asymptote.

VI. DISCUSSION

In C_{2v} symmetry (perpendicular approach of Re^+ and H_2), the most favorable interaction between a transition metal ion and an H_2 molecule occurs when there is an acceptor orbital on the metal ion that interacts with the doubly occupied σ-bonding orbital of H_2 (having a_1 symmetry) and a donor orbital on the metal ion that interacts with the empty σ^*-antibonding orbital of H_2 (having b_2 symmetry). These interactions effectively weaken and lengthen the H_2 bond while simultaneously building electron density between the metal and H atoms. Given this picture, the qualitative characteristics of the potential energy surfaces in Fig. 4 can be readily appreciated. In C_{2v} symmetry, the valence orbitals on Re^+ are $a_1(s)$, $a_1(dz^2)$, $b_2(dxz)$, $b_1(dyz)$, $a_1(dx^2-y^2)$, and $a_2(dxy)$, where the xz plane contains the three atoms and the z axis defines the symmetry axis. In its $^7S(6s^15d^5)$ state, Re^+ has no acceptor orbital such that the interaction with H_2 is largely repulsive, except for a shallow electrostatic well. To empty an orbital, Re^+ must promote to a low-spin state. A favorable interaction is achieved by $Re^+(^5D,5d^6)$, where the empty $6s$ orbital can now act as the acceptor forming an a_1 bonding orbital of ReH_2^+ by combining with the doubly occupied sigma orbital on H_2. Other configurations, $^5S(6s^15d^5)$ and $^5D(6s^25d^4)$ will mix with this state by using $s-d$ hybridization upon interaction with H_2 and therefore need not be considered separately. The most favorable interaction between $Re^+(^5D,5d^6)$ and H_2 is achieved when the $b_2(dxz)$ orbital is the doubly occupied one, as this doubly occupies the b_2 bonding orbital on ReH_2^+. This $a_1^1b_2^2b_1^1a_1^1a_2^1$ atomic configuration leads to the $^5B_2$ surface of Fig. 4. If the "extra" electron is put in the $a_1(dx^2-y^2)$, $a_2(dxy)$, or $b_1(dyz)$ nonbonding orbital, this leads to the $^5A_1$, $^5A_2$, or $^5B_1$ surfaces, respectively, which are much higher in energy because the favorable backbonding interaction of the b_2 orbital is reduced. The $^3B_2$ state has the same configuration as the $^5B_2$, but the low-spin coupling leads to a higher energy according to Hund's rules. For the $^3A_2$ and $^3B_1$ surfaces, the lower spin allows electron density to move out of one of the a_1 orbitals such that the interaction with $\sigma(H_2)$ is less repulsive than for the quintet states. For the $^3A_1$ surface, both a_1 orbitals are still occupied such that it lies slightly higher than these other triplet surfaces.

Alternatively, the metal ion and H_2 can approach one another in a collinear fashion. Indeed, reactions of H_2 with the first row congener of Re^+, Mn^+, are believed to occur primarily by reaction along a collinear surface. This is the more favorable reaction pathway if the acceptor orbital, the valence s or $d\sigma$ orbitals are occupied, in analogy with the $H+H_2$ reaction.

Both Re^+ and Mn^+ have ^7S ground states with $ns^1(n-1)d^5$ configurations, but despite this similarity, the reactivity with dihydrogen is quite distinct. Whereas the threshold for the reaction with $Re^+(^7S)$ appears to correspond to the thermodynamic limit, $Mn^+(^7S)$ exhibits what we have called "impulsive" reactivity in which the threshold is shifted to

much higher energies.[3,4,14,17,18,51] This leads to a maximum cross section for $Mn^+(^7S)$ of only 0.1×10^{-16} cm^2 at 9 eV, essentially twice $D_0(H_2)$.[11,14] This dramatic difference cannot be explained by differences in the reaction endothermicities, 2.18±0.07 eV for $Re^+(^7S)$ versus 2.42±0.14 eV for $Mn^+(^7S)$.[11] Indeed, reaction of $Mn^+(^5S)$ behaves much more like the $Re^+(^7S)$ system, exhibiting a threshold that rises from the thermodynamic limit and a maximum cross section occurring at the energy expected for the analogue of reaction (3) including the electronic energy available.[11] Further comparison of the group 7 metal ions is facilitated by examining the reaction mechanisms as revealed by the studies with HD.

Previous work on the first-row and second-row transition metal cations indicates that the product branching ratio in the reaction of M^+ with HD is very sensitive to the reaction mechanism.[3,4,14,17,18,51] Three categories of reactivity have been established for the first-row transition metal cations and depend on their electron configuration and spin state of metal ions. (1) If M^+ has an electron configuration with empty $4s$ and $3d\sigma$ orbitals, such as for a $3d^x$ configuration where $x<5$, the reaction is efficient and may proceed by an insertion mechanism. These processes are characterized by a product branching ratio in the HD system, $\sigma(MH^+ + D)/\sigma(MD^+ + H)$, that is near unity, consistent with statistical decomposition of a long-lived intermediate. (2) If either the $4s$ or $3d\sigma$ orbital is occupied and the M^+ state is low spin, such as $3d^x$ $(x>5)$ or low-spin coupled $4s^13d^{x-1}$ configurations, the reaction occurs efficiently via a direct mechanism. These processes are characterized by a product branching ratio in the HD system that favors MH^+ by a factor of 2–4, consistent with arguments concerning the conservation of angular momentum.[50,62,66–68] (3) If either the $4s$ or $3d\sigma$ orbital is occupied and the M^+ state is high spin (the highest spin it can possibly have), such as high-spin coupled $4s^13d^{x-1}$ configurations, the reaction is inefficient and tends to react impulsively. These processes are characterized by a product branching ratio in the HD system that favors $MD^+ + H$ by a large factor and exhibits shifts in the thresholds for the H_2 and D_2 systems versus the HD system. Note that these rules are only appropriate for the diabatic reaction behavior, i.e., cases where the electron configuration of the metal ions remains essentially static throughout the course of the reaction.

Results for the reactions of Mn^+ and Re^+ are compared in Fig. 5 in terms of the fraction of metal hydride ion product formed. In accordance with rule 3, $Mn^+(^7S)$ yields much more MnD^+ than MnH^+ over the range shown (indeed at low energies, the observed branching ratio is dominated by small amounts of residual amounts of manganese ion quintet states), characteristic of an impulsive mechanism in the reaction of Mn^+ with HD.[14,17] In contrast, $Mn^+(^5S,^5D)$ states react to form about twice as much MnH^+ as MnD^+ near threshold (close to 1 eV), as expected for a direct process, rule 2. Clearly, $Re^+(^7S)$ does not fall into category 3 nor into category 2, but rather behaves more like category 1, which involves a statistical intermediate. This behavior can be explained as long as this reaction system does not maintain the septet spin as it progresses along the potential energy surface. Coupling of the $^7A_1$ surface that correlates with the ground state reactants to the $^5B_2$ surface provides access to a strongly bound dihydride intermediate that can decompose to $ReH^+(^6\Sigma)+H$ products straightforwardly (Fig. 4). Recent work on the $Re^+(^7S)+CH_4$ system demonstrates that coupling between surfaces of different spin is quite facile for this metal ion,[43] consistent with the observations made here.

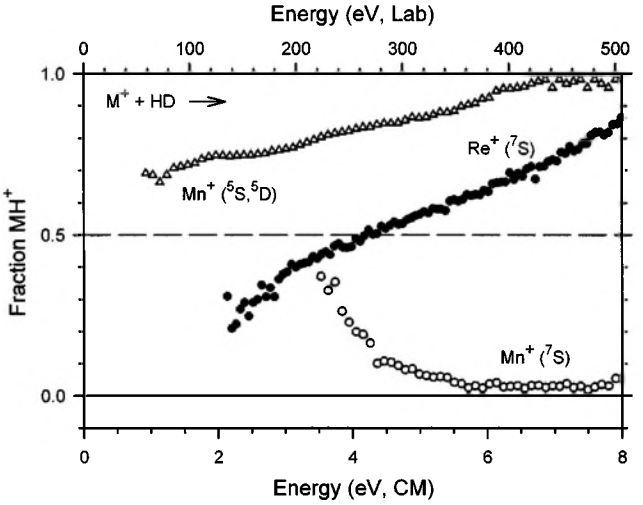

FIG. 5. Product branching fractions ($\sigma_{MH^+}/\sigma_{total}$) for reactions of $Mn^+(^7S)$ (open circles), $Mn^+(^5S/^5D)$ (open triangles), and Re^+ (solid circles) with HD as a function of kinetic energy in the center-of-mass frame.

VII. CONCLUSIONS

Ground state $Re^+(^7S)$ ions are highly reactive with dihydrogen over a wide range of kinetic energies, exhibiting much more efficient reactivity compared with its first-row congener, $Mn^+(^7S)$. Analysis of the kinetic energy dependence of the reaction cross sections provides the BDE of Re^+–H, which is in agreement with *ab initio* calculations when performed using the BHLYP functional or at the QCISD(T) level. As previously elucidated by Holthausen *et al.*,[59] the B3LYP functional overbinds such species by 0.2–0.3 eV and the GVB calculations of Ohanessian *et al.*[29] are too weak by a similar amount. The bond of the $ReH^+(^6\Sigma)$ ground state is stronger than that of the other group 7 metal ion, Mn^+, which is attributed to effective $6s-5d\sigma$ hybridization, a consequence of lanthanide contraction and relativistic effects.[29]

In the Re^+ system, calculations find that reactions with H_2 must occur by coupling surfaces of septet and quintet spin. The branching ratios observed in the Re^++HD reactions indicate that the ground state of Re^+ reacts with dihydrogen largely via a statistical mechanism, which implicates formation of the $^5B_2$ dihydride intermediate. This finding differs greatly from the impulsive mechanism exhibited by $Mn^+(^7S)$ and from the direct mechanism of $Mn^+(^5S)$.[11] This difference can be attributed to efficient coupling between surfaces of different spin, an attribute of this heavy metal system.[43]

ACKNOWLEDGMENT

This work was supported by the National Science Foundation under Grant No. CHE-0135517.

[1] R. H. Crabtree, *The Organometallic Chemistry of the Transition Metals*, 2nd ed. (Wiley, New York, 1994).
[2] G. A. Somorjai, *Introduction to Surface Chemistry and Catalysis* (Wiley, New York, 1994).
[3] P. B. Armentrout, ACS Symp. Ser. **428**, 18 (1990).
[4] P. B. Armentrout, Int. Rev. Phys. Chem. **9**, 115 (1990).
[5] P. B. Armentrout and J. L. Beauchamp, Chem. Phys. **50**, 37 (1980).
[6] P. B. Armentrout and J. L. Beauchamp, J. Am. Chem. Soc. **103**, 784 (1981).
[7] P. B. Armentrout, L. F. Halle, and J. L. Beauchamp, J. Am. Chem. Soc. **103**, 962 (1981).
[8] P. B. Armentrout, L. F. Halle, and J. L. Beauchamp, J. Am. Chem. Soc. **103**, 6501 (1981).
[9] L. F. Halle, F. S. Klein, and Beauchamp, J. Am. Chem. Soc. **106**, 2543 (1984).
[10] M. A. Tolbert and J. L. Beauchamp, J. Am. Chem. Soc. **106**, 8117 (1984).
[11] J. L. Elkind and P. B. Armentrout, J. Chem. Phys. **84**, 4862 (1986).
[12] J. L. Elkind and P. B. Armentrout, J. Phys. Chem. **90**, 6576 (1986).
[13] J. L. Elkind and P. B. Armentrout, Inorg. Chem. **25**, 1078 (1986).
[14] J. L. Elkind and P. B. Armentrout, J. Phys. Chem. **91**, 2037 (1987).
[15] M. L. Mandich, L. F. Halle, and J. L. Beauchamp, J. Am. Chem. Soc. **106**, 4403 (1984).
[16] J. L. Elkind, L. S. Sunderlin, and P. B. Armentrout, J. Phys. Chem. **93**, 3151 (1989).
[17] Y.-M. Chen, J. L. Elkind, and P. B. Armentrout, J. Phys. Chem. **99**, 10438 (1995).
[18] M. R. Sievers, Y.-M. Chen, and P. B. Armentrout, J. Phys. Chem. **100**, 54 (1996).
[19] X.-G. Zhang, C. Rue, S.-Y. Shin, and P. B. Armentrout, J. Chem. Phys. **116**, 5574 (2002).
[20] X.-G. Zhang and P. B. Armentrout, J. Chem. Phys. **116**, 5565 (2002).
[21] P. B. Armentrout, R. V. Hodges, and J. L. Beauchamp, J. Chem. Phys. **66**, 4683 (1977).
[22] P. B. Armentrout, R. V. Hodges, and J. L. Beauchamp, J. Am. Chem. Soc. **99**, 3163 (1977).
[23] P. B. Armentrout and J. L. Beauchamp, Chem. Phys. **48**, 315 (1980).
[24] R. Georgiadis and P. B. Armentrout, J. Phys. Chem. **92**, 7060 (1988).
[25] N. F. Dalleska, K. C. Crellin, and P. B. Armentrout, J. Phys. Chem. **97**, 3123 (1993).
[26] P. B. Armentrout and B. L. Kickel, in *Organometallic Ion Chemistry*, edited by B. S. Freiser (Kluwer, Dordrecht, 1996), p. 1.
[27] P. B. Armentrout, in *Topics in Organometallic Chemistry*, edited by J. M. Brown and P. Hofmann (Springer, Berlin, 1999), Vol. 4-I, p. 1.
[28] P. B. Armentrout, Int. J. Mass. Spectrom. **200**, 219 (2000).
[29] G. Ohanessian, M. J. Brusich, and W. A. Goddard III, J. Am. Chem. Soc. **112**, 7179 (1990).
[30] K. Balasubramanian and D. Dai, J. Chem. Phys. **93**, 7243 (1990).
[31] K. K. Das and K. Balasubramanian, J. Chem. Phys. **94**, 3722 (1991).
[32] D. Dai and K. Balasubramanian, J. Chem. Phys. **95**, 4284 (1991).
[33] D. Dai and K. Balasubramanian, Chem. Phys. Lett. **185**, 165 (1991).
[34] D. G. Dai, W. Cheng, and K. Balasubramanian, J. Chem. Phys. **95**, 9094 (1991).
[35] K. Balasubramanian and Z. Ma, J. Phys. Chem. **95**, 9794 (1991).
[36] H. Zhang and K. Balasubramanian, J. Phys. Chem. **96**, 6981 (1992).
[37] S. K. Loh, D. A. Hales, L. Lian, and P. B. Armentrout, J. Chem. Phys. **90**, 5466 (1989).
[38] R. H. Schultz and P. B. Armentrout, Int. J. Mass Spectrom. Ion Processes **107**, 29 (1991).
[39] E. Teloy and D. Gerlich, Chem. Phys. **4**, 417 (1974).
[40] D. Gerlich, Adv. Chem. Phys. **82**, 1 (1992).
[41] K. M. Ervin and P. B. Armentrout, J. Chem. Phys. **83**, 166 (1985).
[42] P. J. Chantry, J. Chem. Phys. **55**, 2746 (1971).
[43] M. M. Armentrout, F.-X. Li, and P. B. Armentrout, J. Phys. Chem. A (to be published).
[44] B. L. Kickel and P. B. Armentrout, J. Am. Chem. Soc. **117**, 4057 (1995).
[45] D. E. Clemmer, Y.-M. Chen, F. A. Khan, and P. B. Armentrout, J. Phys. Chem. **98**, 6522 (1994).
[46] C. L. Haynes and P. B. Armentrout, Organometallics **13**, 3480 (1994).
[47] B. L. Kickel and P. B. Armentrout, J. Am. Chem. Soc. **117**, 764 (1995).
[48] C. E. Moore, *Atomic Energy Levels*, NSRDS-NBS p. 35, Vol. 3, (1971).
[49] W. J. Chesnavich and M. T. Bowers, J. Phys. Chem. **83**, 900 (1979).
[50] N. Aristov and P. B. Armentrout, J. Am. Chem. Soc. **108**, 1806 (1986).
[51] P. B. Armentrout, in *Advances in Gas Phase Metal Ion Chemistry*, edited by N. G. Adams and L. M. Babcock (JAI, Greenwich, 1992), Vol. 1, p. 83.
[52] F. Muntean and P. B. Armentrout, J. Chem. Phys. **115**, 1213 (2001).
[53] K. P. Huber and G. Herzberg, *Molecular Spectra and Molecular Structure* (Van Nostrand Reinhold, New York, 1979), Vol. IV.
[54] A. D. Becke, J. Chem. Phys. **98**, 5648 (1993).
[55] C. Lee, W. Yang, and R. G. Parr, Phys. Rev. B **37**, 785 (1988).
[56] M. J. Frisch, G. W. Trucks, H. B. Schlegel *et al.*, GAUSSIAN 98, Revision A.11 (Gaussian, Inc., Pittsburgh PA, 1998).
[57] P. J. Hay and W. R. Wadt, J. Chem. Phys. **82**, 299 (1985).
[58] J. B. Foresman and Æ. Frisch, *Exploring Chemistry with Electronic Structure Methods*, 2nd ed. (Gaussian, Pittsburgh, PA, 1996).
[59] M. C. Holthausen, C. Heinemann, H. H. Cornehl, W. Koch, and H. Schwarz, J. Chem. Phys. **102**, 4931 (1995).
[60] D. Andrae, U. Haeussermann, M. Dolg, H. Stoll, and H. Preuss, Theor. Chim. Acta **77**, 123 (1990).
[61] M. C. Holthausen, M. Mohr, and W. Koch, Chem. Phys. Lett. **240**, 245 (1995).
[62] J. L. Elkind and P. B. Armentrout, J. Phys. Chem. **89**, 5626 (1985).
[63] P. B. Armentrout, in *Gas Phase Inorganic Chemistry*, edited by D. H. Russell (Plenum, New York, 1989), p. 1.
[64] P. B. Armentrout, in *Selective Hydrocarbon Activation: Principles and Progress*, edited by J. A. Davies, P. L. Watson, A. Greenberg, and J. F. Liebman (VCH, New York, 1990), p. 467.
[65] M. E. Weber, J. L. Elkind, and P. B. Armentrout, J. Chem. Phys. **84**, 1521 (1986).
[66] L. S. Sunderlin, N. Aristov, and P. B. Armentrout, J. Am. Chem. Soc. **109**, 78 (1987).
[67] J. D. Burley, K. M. Ervin, and P. B. Armentrout, Int. J. Mass Spectrom. Ion Processes **80**, 153 (1987).
[68] P. B. Armentrout, ACS Symp. Ser. **502**, 194 (1992).